Pergamon

Int. J. Heat Mass Transfer. Vol. 40, No. 6, pp. 1379–1390, 1997

0017–9310/97 $17.00+0.00

PII: S0017–9310(96)00185–8

Laminar flow heat transfer to viscous power-law fluids in double-sine ducts

R. M. MANGLIK and J. DING

Department of Mechanical, Industrial and Nuclear Engineering, University of Cincinnati, Cincinnati, OH 45221-0072, U.S.A.

(*Received* 7 *November* 1995 *and in final form* 23 *May* 1996)

Abstract—Fully developed, constant property, laminar flows of viscous power-law fluids in double-sine shaped ducts are considered. The double-sine cross section represents a limiting inter-plate channel geometry in plate heat exchangers with sinusoidally corrugated plates. The non-Newtonian fluid rheology is described by the power-law or Ostwald–de Waele model, and shear thinning ($n < 1$) as well as shear thickening ($n > 1$) flows are considered. Both fluid flow and convective heat transfer problems under **(T)** and **(H1)** thermal boundary conditions are analyzed. Analytical solutions based on the Galerkin integral method are presented for a wide range of flow behavior index ($0.15 \leqslant n \leqslant 2.5$) and duct aspect ratio ($0.25 \leqslant \gamma \leqslant 4.0$). The effects of fluid rheology (pseudoplasticity or dilatancy), duct geometry, and thermal boundary conditions on the velocity and temperature field, are delineated. Also, isothermal friction factor and Nusselt number results for various conditions are presented, and strategies for predicting fRe and Nu are evaluated. Copyright © 1996 Elsevier Science Ltd.

1. INTRODUCTION

Analytical, numerical or experimental results for laminar flow heat transfer in complex duct geometries are essential for the design and application of compact heat exchangers [1–3]. Of particular interest is the plate heat exchanger (PHE), which has found a wide spectrum of usage in food, pharmaceutical and chemical processing [4, 5], where primarily non-Newtonian fluids are encountered. Many different plate surface corrugation patterns are employed in PHEs that essentially promote enhanced heat transfer, thereby providing close temperature control [4] which is particulary beneficial for processing thermally degradable fluids such as food products and polymeric emulsions.

The most widely used plate surface pattern consists of chevron type corrugations with a sinusoidal profile [4], as shown in Fig. 1. When the chevron inclination angle $\beta = 0°$ in these corrugations, inter-plate flow channels with a double-sine cross section are obtained. In effect, laminar flow heat transfer in a double-sine duct represents a limiting case for the heat transfer enhancement due to chevron or herringbone plates. However, despite the extensive usage and study of PHEs [4], results for laminar non-Newtonian flows in such channels do not appear to have been reported in the literature. This is addressed in the present paper.

Processed food, pharmaceutical, chemical, and biochemical fluid media generally have non-Newtonian characteristics, with a non-linear shear stress-strain rate behavior. Extended reviews of their rheology and thermal-hydraulic performance are given by Bird *et al.* [6], Cho and Hartnett [7], and Irvine and Karni [8], among others. However, much of this research has been directed towards circular tube flows [7, 8], with some recent attempts to refine the results, provide newer insights in the transport phenomena, and address more fundamental issues [9–12]. The literature on laminar forced convective heat transfer to non-Newtonian flows in non-circular ducts is somewhat limited. Results for fully developed heat transfer to power-law fluid flows have been reported for isosceles triangular [13], concentric annular [14], rectangular [15–17] and square [18] duct geometries. Lawal and Mujumdar [19] give solutions for thermally developing laminar flows of pseudoplastic fluids in square, pentagonal, and trapezoidal ducts. More recently, thermal-hydraulic characteristics of pseudoplastic and dilatant fluids in semi-circular [20], cross, circular sector, parallel plate and triangular ducts, among others [21] have been reported.

There also have been a few attempts to develop predictive methods for laminar non-Newtonian flows in irregular ducts [13, 22–23]. For the hydrodynamic problem, Kozicki *et al.* [22] suggest normalizing the geometric and flow behavior index effects by a modified apparent viscosity based Reynolds number (Re^*), thereby relating the results to circular tube flows; a somewhat similar, though simpler method has been adopted by Miller [23]. Cheng [13] has devised a correlation parameter that is based on the geometric constants used by Kozicki *et al.* [22], and it appears to predict the Nusselt number results for isosceles triangular ducts rather well. However, a general applicability of this scheme has not been established.

The shear thinning or shear thickening behavior of non-Newtonian fluids greatly affects their thermal-hydraulic performance. For instance, in pseudoplastic

NOMENCLATURE

- a, b — characteristic dimensions of the duct, Fig. 1 [m]
- a_k, b_k, c_k — coefficients of series solution, equation (10)
- d_h — hydraulic diameter [m]
- f — Fanning friction factor, equation (16)
- **H1** — constant axial wall heat flux with uniform peripheral temperature boundary condition
- K — fluid consistency [$Ns^n\ m^{-2}$]
- n — flow behavior index
- Nu — peripherally averaged Nusselt number, equations (18), (19)
- p — fluid pressure [$N\ m^{-2}$]
- Re_g — generalized Reynolds number, $\rho u_m d_h/\mu_g$, equation (17)
- Re^* — Reynolds number defined in equation (20)
- T, T_b — local and bulk fluid temperature [K]
- **T** — constant axial and peripheral wall temperature boundary condition
- u, u_m — axial and mean velocity [$m\ s^{-1}$]
- U, U_m — dimensionless axial and mean velocity, equation (4b)
- x, y, z — Cartesian coordinates [m]
- X, Y — dimensionless Cartesian coordinates, equation (4a).

Greek symbols

- α — thermal diffusivity [$m^2\ s^{-1}$]
- γ — aspect ratio of the duct cross section, $2b/2a$
- Γ_y — contour of duct cross-section, equation (1)
- Δ_{ij} — symmetrical rate of deformation tensor, equation (1)
- η — dimensionless appraent viscosity, equation (4d)
- θ, θ_b — dimensionless local and bulk temperature, equation (4c)
- λ_n — the nth eigenvalue, equation (15c)
- μ_a — apparent viscosity, equation (2) [$N\ s\ m^{-2}$]
- μ_g — generalized viscosity, $K(u_m/d_h)^{n-1}$ [$N\ s\ m^{-2}$]
- ρ — fluid density [$kg\ m^{-3}$]
- τ, τ_0 — local and perimeter averaged wall shear stress [$N\ m^{-2}$]
- ω — weight function, equations (10), (11).

Subscripts

- H1 — pertaining to the **H1** thermal boundary condition
- max — maximum value
- T — pertaining to the **T** thermal boundary condition.

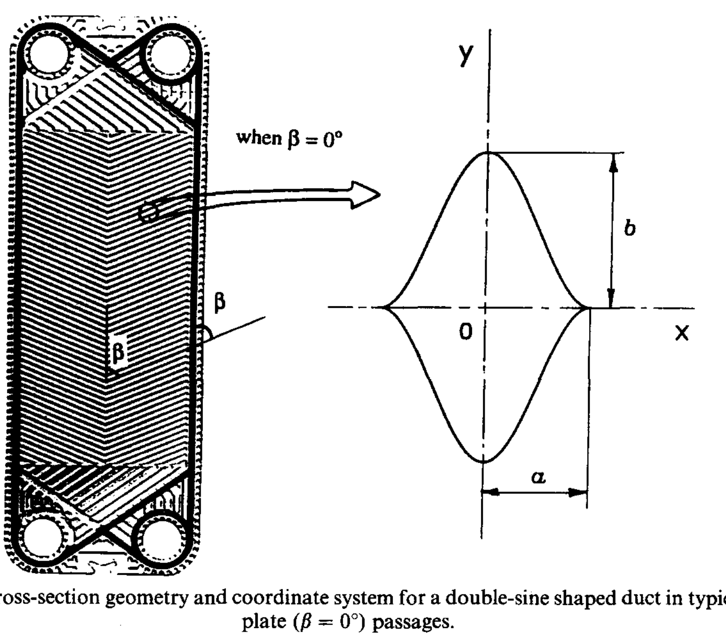

Fig. 1. Flow cross-section geometry and coordinate system for a double-sine shaped duct in typical chevron plate ($\beta = 0°$) passages.

fluids, while the wall shear stress decreases, the temperature gradients tend to increase, thereby enhancing the heat transfer [9, 11]. In contrast, increasing dilatancy tends to exhibit larger wall shear stresses with a deterioration in the heat transfer [11]. These anomalous characteristics are further compounded in flows through irregular cross-section ducts, where the sharp corners of the flow geometry tend to significantly alter the convective behavior. Thus, in the absence of precise friction factor and Nusselt number data for such flows, the effectiveness of the associated thermal processes is greatly compromised. For laminar flows, a regime normally encountered in thermal processing of viscous fluids, issues relating to effects of flow behavior, aspect ratio of the double-sine duct, and wall heating/cooling conditions are addressed in this study. Fully developed flows are considered with both uniform wall temperature (**T**) and uniform wall heat flux (**H1**) boundary conditions; these simulate the most fundamental heating/cooling conditions in practical heat exchangers. The Galerkin integral method [24–25] has been employed to obtain velocity and temperature field solutions. This technique has been successfully applied in the literature to obtain very accurate fRe and Nu results (within $\pm 0.3\%$) for forced convection in a variety of different irregular ducts [26–28]. Isothermal fRe, Nu_T and Nu_{H1} results for a wide range of flow behavior index ($0.15 \leqslant n \leqslant 2.5$) and aspect ratio of the double-sine duct ($0.25 \leqslant \gamma \leqslant 4.0$) are presented, and generalized prediction strategies discussed.

2. MATHEMATICAL ANALYSIS

To model the non-linear shear stress-strain rate relationship, the two-parameter power-law equation of Ostwald–de Waele [6] is employed. This constitute relationship can be expressed in a general form as

$$\tau_{ij} = K\left|\sqrt{\tfrac{1}{2}(\Delta_{ij}:\Delta_{ij})}\right|^{n-1}\Delta_{ij} = \mu_a\Delta_{ij}; \qquad (1)$$

$$\Delta_{ij} = \frac{1}{2}[\nabla\mathbf{v}+(\nabla\mathbf{v})^t] = [(\partial v_i/\partial q_j)+(\partial v_j/\partial q_i)]$$

where K is the fluid consistency, n the flow behavior index, and μ_a the apparent viscosity; $n < 1$ for pseudoplastic fluids, $n > 1$ for dilatant fluids, and $n = 1$ for Newtonian fluids ($K = \mu$). For fully developed flows in a two-dimensional duct and Cartesian coordinates, the apparent viscosity is given by

$$\mu_a = K[(\partial u/\partial x)^2+(\partial u/\partial y)^2]^{(n-1)/2}. \qquad (2)$$

The flow cross-section geometry of the double-sine duct is shown in Fig. 1, where the outer boundary or wall surface contour is described by

$$\Gamma_y = \pm(b/2)[1+\cos(\pi x/a)] \qquad (3)$$

$$-a \leqslant x \leqslant a,\ -b \leqslant y \leqslant b$$

and the aspect ratio is defined as $\gamma = (2b/2a)$. Steady state, constant property, hydrodynamically and thermally fully developed laminar flow of viscous power-law fluids is considered, and body forces, axial conduction, and viscous dissipation are ignored.

In order to nondimensionalize the governing differential equations, the following dimensionless coordinates and variables are introduced:

$$X = (x/2a) \quad Y = (y/2a) \qquad (4a)$$

$$U = u/[(4a^2/\mu_g)(\mathrm{d}p/\mathrm{d}z)] \quad U_m = u_m/[(4a^2/\mu_g)(\mathrm{d}p/\mathrm{d}z)] \qquad (4b)$$

$$\theta = (T_w - T)/[(4a^2u_m/\alpha)(\mathrm{d}T_b/\mathrm{d}z)] \qquad (4c)$$

$$\theta_b = (T_w - T_b)/[(4a^2u_m/\alpha)(\mathrm{d}T_b/\mathrm{d}z)]$$

$$\eta = \mu_a/\mu_g = (d_h/2aU_m)^{n-1}[(\partial U/\partial X)^2 + (\partial U/\partial Y)^2]^{(n-1)/2}. \qquad (4d)$$

Here, u_m is the mean axial velocity, and T_b is the bulk mean temperature. Also, the generalized viscosity μ_g ($=K[u_m/d_h]^{n-1}$) has the virtue of normalizing the results relative to flows in an equivalent circular tube. Thus, the axial momentum and energy conservation statements take on the dimensionless form

$$\eta\left(C_x\frac{\partial^2 U}{\partial X^2}+C_y\frac{\partial^2 U}{\partial Y^2}\right) = 1 \qquad (5)$$

$$\frac{\partial^2\theta}{\partial X^2}+\frac{\partial^2\theta}{\partial Y^2}-\Theta = 0 \quad \Theta = \begin{cases} -(U\theta/U_m\theta_b) & \text{for } \mathbf{T} \\ -(U/U_m) & \text{for } \mathbf{H1} \end{cases} \qquad (6)$$

where the coefficients C_x and C_y are given as

$$C_x(X,Y) = 1+\frac{n-1}{1+\left(\frac{\partial U}{\partial Y}\right)^2\Big/\left(\frac{\partial U}{\partial X}\right)^2}$$

and

$$C_y(X,Y) = 1+\frac{n-1}{1+\left(\frac{\partial U}{\partial X}\right)^2\Big/\left(\frac{\partial U}{\partial Y}\right)^2}.$$

Equations (5) and (6) are subject to the following boundary conditions:

$$U = \theta \quad \theta = 0 \text{ on } \Gamma \qquad (7a)$$

$$U \text{ and } \theta \quad \text{are finite at} \quad \mathrm{X} = \mathrm{Y} = 0. \qquad (7b)$$

The application of Galerkin integral method [24] is based on the requirement that the solution of the governing differential equation correspond to the minimum of the integral

$$I = \iint_{A_c}[\nabla^2\Phi(X,Y)+2f(X,Y)\Phi(X,Y)]\,\mathrm{d}X\,\mathrm{d}Y \qquad (8)$$

over the duct cross section, where Φ is the dependent variable. This functionally seeks a solution of the form

$$\Phi = \sum_{k=1}^{n} G_k \Psi_k(X, Y) \tag{9}$$

such that the homogeneous boundary condition $\Phi = 0$ on Γ is unconditionally satisfied. Here the Galerkin function Ψ is described by (X, Y) and a weight function $\omega(X, Y)$. Correspondingly, the fully developed velocity and temperature field solutions given by equation (9) can be expressed as

$$U = \omega(X, Y)(a_1 + a_2X^2 + a_3Y^2 + a_4X^4 + a_5X^2Y^2 + a_6Y^4 + \dots) \tag{10a}$$

$$\theta_{\mathrm{T}} = \omega(X, Y)(b_1 + b_2X^2 + b_3Y^2 + b_4X^4 + b_5X^2Y^2 + b_6Y^4 + \dots) \tag{10b}$$

$$\theta_{\mathrm{H1}} = \omega(X, Y)(c_1 + c_2X^2 + c_3Y^2 + c_4X^4 + c_5X^2Y^2 + c_6Y^4 + \dots) \tag{10c}$$

where the coefficients G_k are designated as a_k, b_k, and c_k for the respective field variables $\Phi = U$, θ_{T}, and θ_{H1}. The weight function is obtained from a combination of trigonometric functions of (X, Y), such that it is continuous together with its first and second derivatives. For the double-sine duct geometry (Fig. 1) it is expressed as

$$\omega(X, Y) = [Y + (\gamma/4)(1 + \cos 2\pi X)] \times [Y - (\gamma/4)(1 + \cos 2\pi X)]. \tag{11}$$

Note that $\omega(X, Y) = 0$ on Γ, and it is continuous and twice differentiable; additional details on the selection of ω can be found in ref. [29].

By invoking Green's theorem for the Euler–Lagrange equation problem, the minimum value problem of the integral of the Poisson-type governing differential equation is equivalent to

$$\iint_{A_c} [\nabla^2\Phi - f(X, Y)]\Psi_i \, \mathrm{d}X \, \mathrm{d}Y = 0 \tag{12a}$$

where

$$f(X, Y) = \begin{cases} 1 & \Phi = U \\ -(U\theta/U_{\mathrm{m}}\theta_{\mathrm{b}}) & \Phi = \theta_{\mathrm{T}} \\ -(U/U_{\mathrm{m}}) & \Phi = \theta_{\mathrm{H1}} \end{cases}. \tag{12b}$$

Equation (12) thus provides the system of equations that describe the coefficients G_k (or a_k, b_k, and c_k, as the case may be). For the velocity problem, with the substitution of equation (10a) into equation (12), the system of equations for coefficients a_k is obtained as

$$\sum_{k=1}^{n} a_k \iint_{A_c} \int \eta \left(C_x \frac{\partial^2 \Psi_k}{\partial X^2} + C_y \frac{\partial^2 \Psi}{\partial Y^2} \right) \Psi_i \, \mathrm{d}X \, \mathrm{d}Y = \iint_{A_c} \Psi_i \, \mathrm{d}X \, \mathrm{d}Y. \tag{13}$$

Similarly, for the temperature problem with **H1** boundary condition, by combining equations (10c) and (12), the system of equations for evaluating the coefficients c_k is

$$\sum_{k=1}^{n} c_k \iint_{A_c} \left(\frac{\partial^2 \Psi_k}{\partial X^2} + \frac{\partial^2 \Psi_k}{\partial Y^2} \right) \Psi_i \, \mathrm{d}X \, \mathrm{d}Y = -\int_{A_c} \iint (U/U_{\mathrm{m}}) \Psi_i \, \mathrm{d}X \, \mathrm{d}Y. \tag{14}$$

For the **T** boundary condition, however, substituting equation (10b) in equation (12) yields

$$\sum_{k=1}^{n} b_k \iint_{A_c} \Psi_i \nabla^2 \Psi_k \, \mathrm{d}X \, \mathrm{d}Y + \sum_{k=1}^{n} (b_k/\theta_{\mathrm{b}}) \iint_{A_c} (U/U_{\mathrm{m}}) \Psi_i \Psi_k \, \mathrm{d}X \, \mathrm{d}Y = 0 \tag{15a}$$

which is an eigenvalue problem that can be expressed in matrix form as

$$[\hat{A}]\{B\} + [\hat{C}]\{B'\} = 0. \tag{15b}$$

Note that the elements of $\{B'\}$ are $b'_k = (b_k/\theta_{\mathrm{b}})$. The solution of equation (15b) is of the form

$$\{B\} = b_1\{d_1\}\mathrm{e}^{\lambda_1 z} + b_2\{d_2\}\mathrm{e}^{\lambda_2 z} + \dots + b_n\{d_n\}\mathrm{e}^{\lambda_n z} \tag{15c}$$

where λ_ns are the eigenvalues that are obtained by solving $\det|\hat{A} + \lambda\hat{C}| = 0$, and they are all negative if the matrix $[\hat{C}]$ is finite and positive; $\{d_n\}$ are the corresponding eigenvectors. Also, elements of the coefficient matrices $[\hat{A}]$ and $[\hat{C}]$ in equation (15b) are obtained from

$$\alpha_{ik} = \iint_{A_c} \Psi_i \nabla^2 \Psi_k \, \mathrm{d}X \, \mathrm{d}Y$$

and

$$\hat{c}_{ik} = \iint_{A_c} (U/U_{\mathrm{m}}) \Psi_i \Psi_k \, \mathrm{d}X \, \mathrm{d}Y.$$

After determining the fully developed velocity and temperature distributions in the double-sine flow cross-section, the corresponding isothermal friction factor and Nusselt number (for both **T** and **H1** conditions) can be calculated. Based on a force balance across an element of the duct cross-section and its definition, the Fanning friction factor for power-law fluids is given by

$$fRe_{\mathrm{g}} = -[(d_{\mathrm{h}}/2a)^2]/(2U_{\mathrm{m}}) \tag{16}$$

where the generalized Reynolds number Re_{g} is defined as

$$Re_{\mathrm{g}} = (\rho u_{\mathrm{m}} d_{\mathrm{h}}/\mu_{\mathrm{g}}) = (\rho u_{\mathrm{m}}^{2-n} \mathrm{d}_{\mathrm{h}}^{n}/K). \tag{17}$$

For the peripherally averaged Nusselt number, the usual hydraulic diameter based definition is employed.

With fully developed flow and the **T** boundary condition, the contribution of all eigenvalues, except λ_1, diminishes. Consequently, the Nusselt number can be calculated as

$$Nu_{\mathrm{T}} = -(\lambda_1/4)(d_{\mathrm{h}}/2a)^2. \tag{18}$$

In the case of the **H1** boundary condition, the Nusselt number is obtained from

$$Nu_{\mathrm{H1}} = [(d_{\mathrm{h}}/2a)^2]/(4\theta_{\mathrm{b}}). \tag{19}$$

With the numerical computations of a_k, b_k, c_k, and λ_k, the velocity and temperature distributions, and isothermal friction factors and Nusselt numbers can be evaluated from equations (10), (16)–(19), for different aspect ratios of the duct cross section and flow behavior index. These were carried out by using standard numerical techniques [29], with the number of terms and coefficients in the series expansion selected such that the maximum error was less than 0.01%, relative to the solution with larger number of terms. The friction factor, Nusselt number and peak values of velocity and temperature profiles attain virtually constant values as the number of terms increase, thereby indicating convergent solutions. In general, 6–21 terms were required in the series expansions, with more number of terms needed as γ increases. Additional details of the methodology and accuracy are given in ref. [29]. The validity and accuracy of the present results and solution technique were established by calculating friction factor and Nusselt number results for Newtonian flows in sine ducts, and comparing them with those given in ref. [1]. As presented elsewhere [28], there was excellent agreement between the two; additional comparisons have been made with results for triangular and rhombic ducts, that are qualitatively similar.

3. RESULTS AND DISCUSSION

Analytical solutions based on the Galerkin integral method for fully developed laminar power-law fluid flow and heat transfer in double-sine shaped ducts are presented for a wide range of duct aspect ratios, $0.25 \leqslant \gamma \leqslant 4.0$, and flow behavior indices, $0.15 \leqslant n \leqslant 2.5$. Both local (velocity and temperature) and global (friction factor and Nusselt number) results are given, that highlight the effects of duct geometry, flow behavior index, and wall thermal boundary conditions (**T** and **H1**).

3.1. *Velocity and temperature fields*

The shear behavior of a viscous non-Newtonian fluid, as represented by the power-law index n, has a strong influence on laminar flow axial velocity distribution. This is seen from Fig. 2, where isovelocity (u/u_{m}) contours for typical pseudoplastic ($n = 0.15$), Newtonian ($n = 1.0$), and dilatant ($n = 2.5$) flows in a double-sine duct of aspect ratio $\gamma = 1.0$ are presented. As seen from the isovelocity maps, relative to Newtonian flows, shear thinning fluids ($n = 0.15$) tend to have a flat, plug flow like velocity profile, whereas shear thickening fluids ($n = 2.5$) tend to have a sharper conical profile with a higher peak or centerline velocity. Also presented in Fig. 2 are the corresponding isotherm $(\theta/\theta_{\mathrm{b}})$ maps for the **T** and **H1** thermal boundary conditions, and the effect of flow behavior index on the thermal field is evident from these plots. As would be expected, pseudoplastic fluids ($n < 1$) tend to have a somewhat flatter temperature profile in the core of the duct with relatively higher gradients near the wall. Dilatant flows ($n > 1$), on the other hand, are characterized by sharper core-region profiles with smaller wall-region gradients.

The effects of duct aspect ratio γ on the velocity and temperature fields are shown in Fig. 3. Here, isovelocity (u/u_{m}) contours and the respective isotherms $(\theta/\theta_{\mathrm{b}})$ for **T** and **H1** conditions are presented for flows with $n = 1$ in double-sine ducts with $\gamma = 0.25$ and 4.0. Because of the 'squeezing' effect of the channel geometry, higher peak or centerline velocities are obtained when compared with flows in a duct of $\gamma = 1$. While higher centerline velocities produce greater fluid mobility in the core portion because of the narrowing of the duct cross section ($\gamma < 1$ or $\gamma > 1$), the flow tends to stagnate in the sharp or narrow corner regions. As a result, local thermal hot or cold flow regions are obtained in the corner sections of the duct. Much of the fluid in the corner tends to attain the wall temperature in fully developed flows, with significantly cooler or hotter temperature in the core flow. This thermal maldistribution is much larger for the **T** boundary condition as compared with the **H1** condition. In the latter case, the wall temperature is higher and 'runs away' from the fluid local and bulk temperatures, whereas with the **T** condition the fluid local/bulk temperatures approach the wall condition as the flow becomes fully developed. In any event, this inhomogeneity in the flow and temperature field is particularly detrimental for thermal processing of food and biochemical products; such conditions would lead to inefficient processing and thermal degradation of the fluid product.

The deviation from Newtonian behavior and the effect of duct shape are further illustrated in terms of the temperature difference $[(\theta/\theta_{\mathrm{b}})_n - (\theta/\theta_{\mathrm{b}})_{n=1}]$ on the mid-plane ($y = 0$) for typical flow conditions in Fig. 4. The distortions in the temperature field due to the shear thinning or shear thickening flow behavior are clearly evident in Fig. 4. Primarily because of plug-like flows in highly shear-thinning fluids, as seen from Fig. 4(a), the deviations in the core region temperature distributions become very pronounced with increasing γ. In highly shear-thickening fluids, on the other hand, these deviations are much larger in the middle region between the core and corners of the duct. This is seen in Fig. 4(b), and can be attributed to the conical flow behavior of dilatant fluids. Also, the wall–fluid temperature differences are smaller in this case, relative

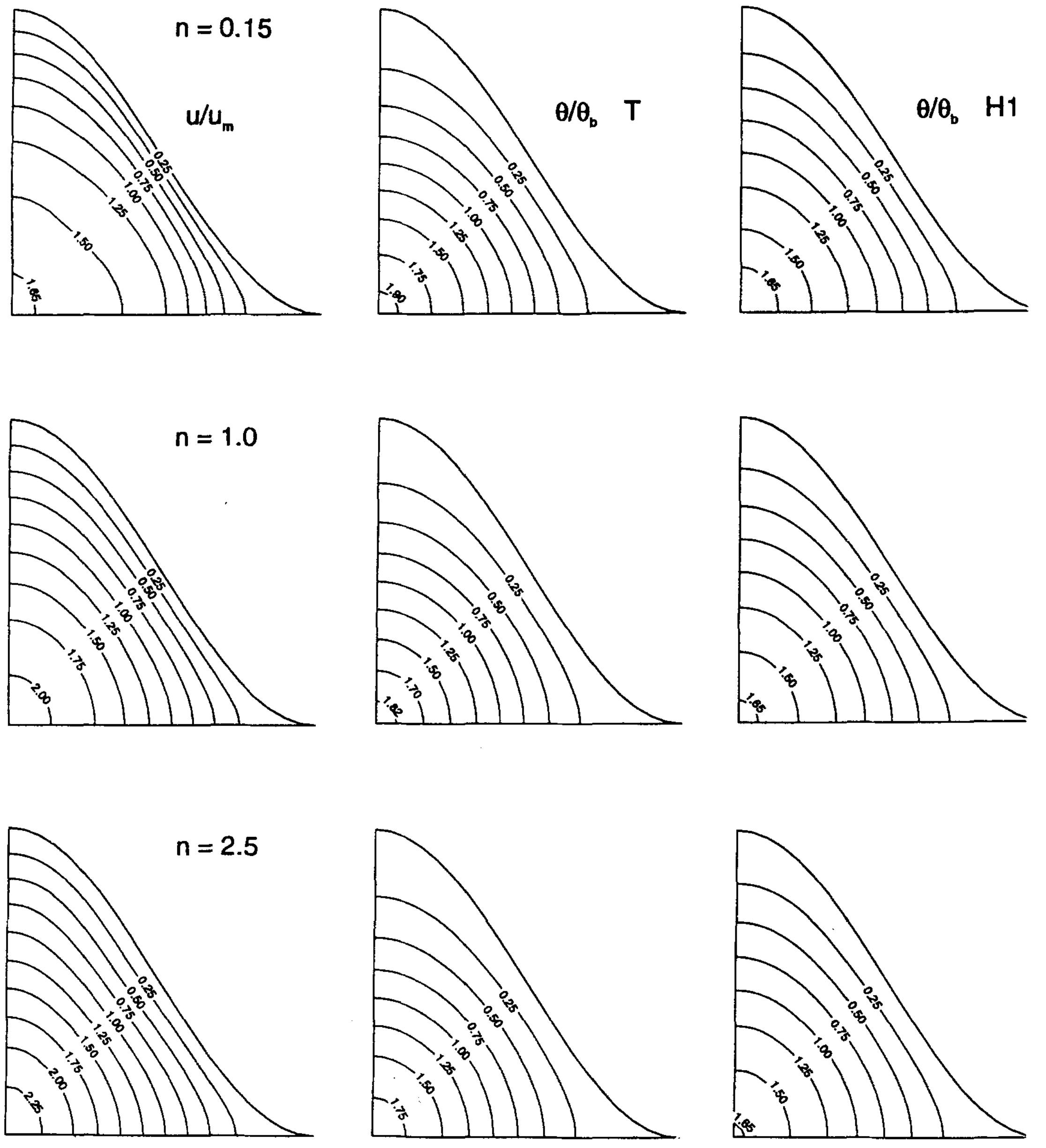

Fig. 2. Axial velocity (u/u_m) contours and isotherm (θ/θ_b) maps for $n = 0.15$, 1.0 and 2.5 in a double-sine duct with $\gamma = 1.0$.

to Newtonian fluids, but are much larger in pseudoplastic flows.

The complex flow behavior due to non-Newtonian and duct geometry effects is also reflected in the wall shear stresses, and this is graphically depicted in Fig. 5. The effect of fluid rheology on laminar flows in a double-sine channel with $\gamma = 1.0$ is shown in Fig. 5(a) in terms of (τ_w/τ_0); τ_w is the local wall shear stress and τ_0 is the average wall shear stress. With plug-like uniform velocity distributions in pseudoplastic fluids $(n < 1)$, in comparison with Newtonian flows, the wall shear stresses (τ_w/τ_0) are uniformly distributed along the duct surface. The relatively elongated or conical flow profiles due to the shear thickening characteristics of dilatant fluids $(n > 1)$, however, produce large variations in (τ_w/τ_0). The lower mid-surface between the peak and valley of the sinusoidal wall profile sees the highest shear stresses, with much smaller values at the apex. Similar effects are also obtained when the duct aspect ratio is varied, and the influence of aspect ratio ($\gamma = 0.25$, 1.0, and 4.0) on (τ_w/τ_0) is illustrated in Fig. 5(b). For $\gamma < 1$, (τ_w/τ_0) tends to become more uniformly distributed along the wall. On the contrary, flows in $\gamma > 1$ ducts generate large variations in wall shear stress, with peak values near the $(x/2a) \approx 0.3$ portion of the duct geometry.

3.2. *Friction factor and Nusselt number*

Isothermal friction factor results for double-sine ducts with $\gamma = 0.25$, 0.5, 1.0, 2.0 and 4.0, and non-

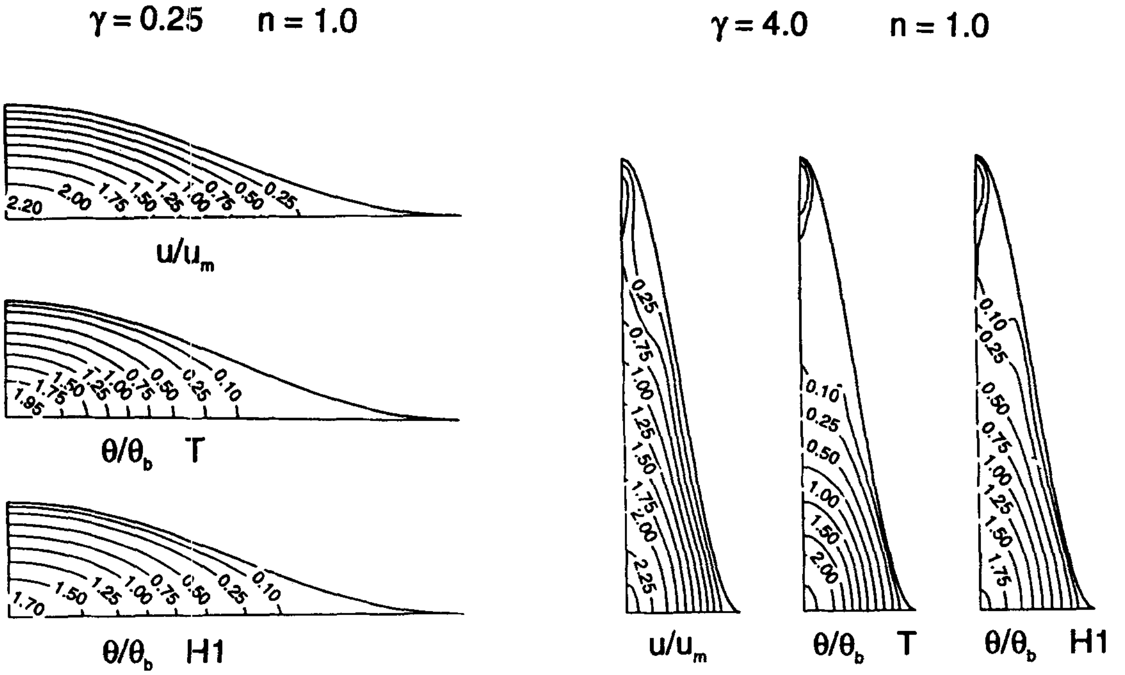

Fig. 3. Axial velocity (u/u_m) contours and isotherm (θ/θ_b) maps for $n = 1.0$ in double-sine ducts with $\gamma = 0.25$ and 4.0.

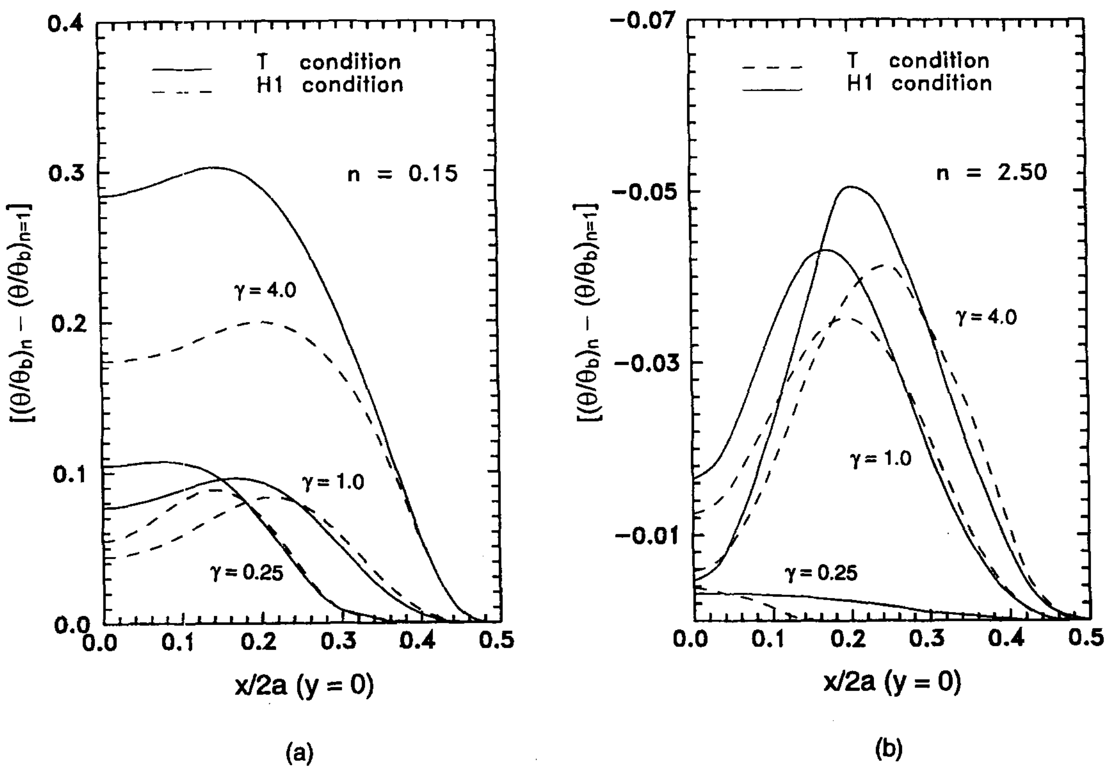

Fig. 4. Effect of flow behavior index on the mid-plane ($y = 0$) temperature difference $[(\theta/\theta_b)_n - (\theta/\theta_b)_{n=1}]$ distribution under **T** and **H1** boundary conditions: (a) for $n = 0.15$ and (b) for $n = 2.5$.

Newtonian flows with different flow behavior indices ($0.15 \leqslant n \leqslant 2.5$) are given in Table 1. Also tabulated are the values of maximum or peak centerline velocities in terms of (u_{max}/u_{min}) for each case. As discussed earlier, the latter listing quantitatively demonstrates the 'squeezing' effect of decreasing/increasing duct aspect ratio on power-law fluid flows. Higher peak velocities are obtained when $\gamma < 1$

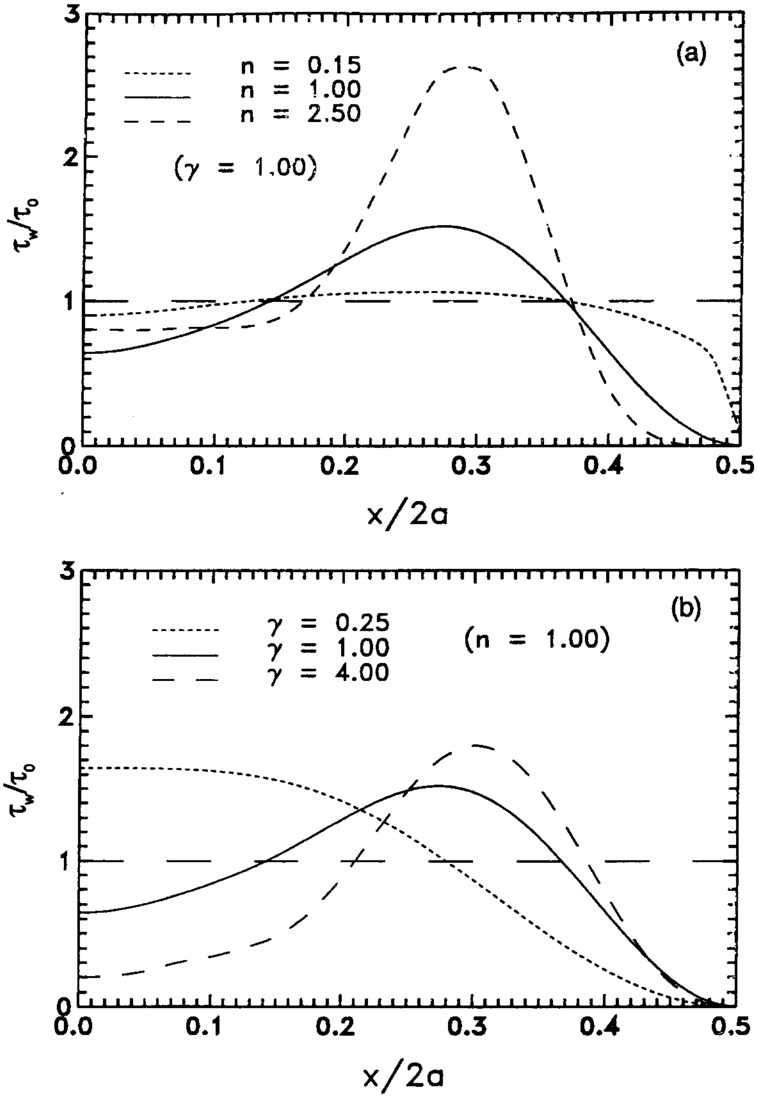

Fig. 5. Wall shear stress distribution (τ_w/τ_0) in double-sine ducts: (a) variation with n and (b) variation with γ.

Table 1. Fully developed laminar power-law fluid flow characteristics in double-sine ducts

n	0.15	0.40	0.60	0.80	1.00	1.20	1.50	2.00	2.50
					$\gamma = 0.25$				
u_{max}/u_m	1.6922	1.9127	2.0583	2.1625	2.2284	2.2730	2.3129	2.3683	2.3968
fRe_g	2.6782	3.7812	5.2209	7.2724	10.256	14.446	24.135	56.636	132.96
					$\gamma = 0.50$				
u_{max}/u_m	1.6885	1.7766	1.9245	2.0349	2.1157	2.1769	2.2452	2.3222	2.3728
fRe_g	3.1230	4.5011	6.0271	8.2064	11.440	15.920	26.254	60.867	142.04
					$\gamma = 1.00$				
u_{max}/u_m	1.6674	1.7397	1.8840	1.9974	2.0809	2.1452	2.2194	2.3082	2.3718
fRe_g	3.3107	5.1435	6.9306	9.5553	13.348	18.765	31.482	75.234	180.79
					$\gamma = 2.00$				
u_{max}/u_m	1.7873	1.8148	1.9863	2.1184	2.2144	2.2858	2.3648	2.4534	2.5119
fRe_g	2.7656	4.7203	6.7369	9.9555	14.860	22.233	40.598	109.28	281.99
					$\gamma = 4.00$				
u_{max}/u_m	1.8165	2.0204	2.2249	2.3623	2.4481	2.5006	2.5515	2.6010	2.6303
fRe_g	1.6509	3.3125	5.7891	9.6492	15.413	24.097	46.023	129.83	353.76

or $\gamma > 1$ for all n. The isothermal friction factor results indicate that fRe_g generally increases with n. For example, in a double-sine duct with $\gamma = 1$, fRe_g varies from 3.3107 for $n = 0.15$ to 180.79 for $n = 2.5$; this trend is seen for all aspect ratio ducts. When considering the combined effects of n and γ, however, with $n < 0.8$, i.e. highly shear-thinning fluids, the maximum fRe_g is obtained for $\gamma = 1$. This is not uncharacteristic of flows in irregular duct geometries with sharp edges, where the 'corners' greatly affect the fluid mobility. In Newtonian flows in isosceles triangular and rhombic ducts, for example, peak value of fRe is obtained when $\gamma \cong 1$ [1]. Similarly, fRe vs γ variations in eccentric annuli and narrow annular-sector ducts exhibit maxima and/or minima at intermediate aspect ratios [1]. On the other hand in trapezoidal ducts, fRe for Newtonian flows is minimum for $\gamma \cong 1$, and it tends to attain the value for parallel plate flows as $\gamma \to 0$ or ∞; extended comparisons and discussion are presented in ref. [28]†. For slightly pseudoplastic ($n = 0.8$), Newtonian ($n = 1.0$), and dilatant ($n > 1$) fluids, fRe_g increases with increasing aspect ratio.

There have been few attempts at developing generalized correlations for non-Newtonian flows [22, 23]. Of these, by normalizing hydrodynamic characteristics with those of Newtonian flows in circular tubes, Kozicki *et al.* [22] have suggested that friction factors in irregular ducts can be predicted by

$$fRe^* = 16 \quad Re^* = \frac{\rho u_m^{2-n} d_h^n}{8^{n-1} K[(a+bn)/n]^n} \tag{20}$$

where a and b are geometric constants that depend upon the duct shape. This expression is supposedly valid for any power-law index $n > 0$, and the relationship between fRe_g and fRe^* is as follows:

$$\frac{fRe_g}{fRe^*} = 2^{3n-3}\left(\frac{a+bn}{n}\right)^n. \tag{21}$$

A comparison of the present study's results with fRe^* predictions of Kozicki *et al.* [22] is presented in Fig. 6. As is evident, there is reasonable agreement only for near unity values of n ($0.6 \leqslant n \leqslant 1.5$), i.e. moderately pseudoplastic or dilatant fluids. For $n < 0.6$ or $n > 1.5$, equation (20) fails to provide adequate predictions; for dilatant fluids and ducts with $\gamma = 4$ particularly, the disagreement is quite large. This is not unexpected, given that sharp corners in the duct's cross-section geometry greatly influence the flow field, and more so in very small/large aspect ratio ducts. Even in the original treatment of Kozicki *et al.* [22], for example, 17%–25% deviations were observed in fRe^* predictions for concentric annuli with very small inner cylinder radii. As such, in the present case, the Kozicki *et al.* [22] scheme should be generalized and extended to highly shear-thinning or shear-thickening fluid flows and sharp-cornered channels with caution.

For the thermal problem, non-Newtonian effects are further highlighted by the maximum centerline-to-wall temperature differences (θ_{max}/θ_b). These are tabulated in Tables 2 and 3, respectively, for **T** and **H1** boundary conditions. Reflecting the flow behavior, the centerline-to-wall temperature difference increases with increasing pseudoplasticity ($n < 1$); the converse is true for increasing dilatancy ($n > 1$), and (θ_{max}/θ_b) decreases. This holds for both **T** and **H1** conditions, though relatively smaller values are obtained with the latter boundary condition. Furthermore, because of the flow 'squeezing' when $\gamma < 1$ or $\gamma > 1$, higher (θ_{max}/θ_b) values are obtained for shear-thinning or shear-thickening flows with the same n. The corresponding Nusselt numbers for the **T** and **H1** thermal boundary conditions are also listed in Tables 2 and 3, respectively. The results clearly demonstrate that shear-thinning flows with higher wall temperature gradients enhance heat transfer, whereas shear-thickening flows lead to a deterioration in heat transfer. Furthermore, irrespective of the thermal boundary condition and flow behavior index, as the duct aspect ratio γ increases from 0.25 to 4.0, Nu increases up to $\gamma = 1.0$ and then decreases with further increase in γ. That is, the peak value of Nu is obtained for a double-sine shaped duct with an aspect ratio of unity. Also, consistent with the influence of wall boundary conditions, $Nu_{H1} > Nu_T$ for any flow behavior index n and duct aspect ratio γ.

In an attempt to provide a general prediction of heat transfer in non-circular cross-section ducts with any type of boundary condition, Cheng [13] has proposed the following correlations:

$$(Nu)_n = \left[\frac{(a+bn)}{(a+b)n}\right]^{1/3} (Nu)_{n=1}. \tag{22}$$

Here a and b are the same geometric constants as those developed for isothermal flow by Kozicki *et al.* [22]. Comparisons with the present study's results for double-sine ducts with **T** and **H1** boundary conditions are presented in Fig. 7. This figure shows the results for variations in both the flow behavior index n and duct aspect ratio γ. With the exception of $n = 0.15$, there is good agreement between the predictions and present results. This is not surprising given that Cheng [13] has formulated the correlation on the basis of isosceles triangular ducts [8], a shape that is somewhat similar to a sine profile.

4. CONCLUSIONS

For constant property, fully developed laminar flows of power-law fluids in double-sine shaped ducts, solutions for both **T** and **H1** boundary conditions

† It may be noted that the analytical results for Newtonian flows given in ref. [28] are for double half-sine ducts, i.e. the duct's boundaries are described by mirror images of a half-sine wave. In the present case, the shape is a full sine wave, which is a more appropriate model for inter-plate channels in plate heat exchangers.

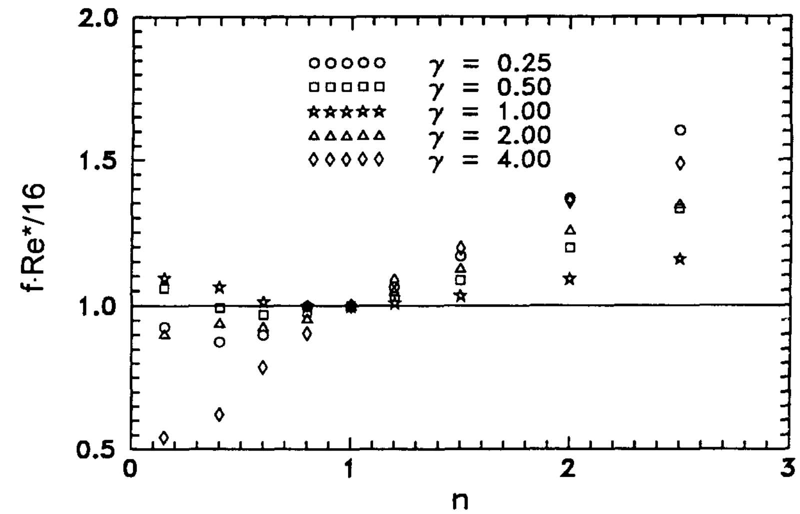

Fig. 6. Comparison of present results with fRe^* predictions of Kozicki *et al.* [22] for fully developed laminar flows with different flow behavior index n in double-sine ducts.

Table 2. Fully developed laminar power-law fluid flow heat transfer characteristics in double-sine ducts with the **T** thermal boundary condition

n	0.15	0.40	0.60	0.80	1.00	1.20	1.50	2.00	2.50
					$\gamma = 0.25$				
θ_{max}/θ_b	2.1429	2.0712	2.0506	2.0400	2.0381	2.0376	2.0366	2.0353	2.0349
Nu_T	2.1116	1.9370	1.8727	1.8434	1.8245	1.8145	1.8037	1.7932	1.7908
					$\gamma = 0.50$				
θ_{max}/θ_b	1.9290	1.9078	1.8749	1.8620	1.8538	1.8524	1.8475	1.8397	1.8363
Nu_T	2.6702	2.4943	2.4374	2.3787	2.3422	2.3143	2.2867	2.2506	2.2315
					$\gamma = 1.00$				
θ_{max}/θ_b	1.9281	1.8964	1.8744	1.8608	1.8512	1.8508	1.8453	1.8367	1.8347
Nu_T	3.1671	3.0604	2.9471	2.8786	2.8361	2.7865	2.7509	2.7149	2.6814
					$\gamma = 2.00$				
θ_{max}/θ_b	2.1277	2.0969	2.0680	2.0500	2.0488	2.0470	2.0398	2.0354	2.0281
Nu_T	3.0326	2.9980	2.9453	2.8473	2.7660	2.7093	2.6586	2.6237	2.6183
					$\gamma = 4.00$				
θ_{max}/θ_b	2.6682	2.5235	2.4712	2.3910	2.3841	2.3837	2.3820	2.3804	2.3794
Nu_T	2.8011	2.5563	2.4353	2.3710	2.2941	2.2873	2.2822	2.2709	2.2630

are obtained by the Galerkin function based integral method. Results for velocity and temperature distributions, and the corresponding values of fRe_g, Nu_T, and Nu_{H1} with varying flow behavior index ($0.15 \leqslant n \leqslant 2.5$) in double-sine ducts of different aspect ratios ($0.25 \leqslant \gamma \leqslant 4.0$) illustrate the following:

(1) Larger peak velocities and wall-to-centerline fluid temperature differences are obtained in small and large aspect ratio ducts ($\gamma < 1$ or $\gamma > 1$), with sharper gradient changes in the respective distributions. In shear-thinning fluids ($n < 1$), flatter plug-like velocity profiles are obtained, and in shear-thickening fluids ($n > 1$), sharper and almost conical profiles are obtained. As a consequence, there is considerable deviation in the temperature profiles. In the former case, the core region flow has higher temperatures, compared with Newtonian fluids. The converse is true in dilatant fluids, with larger maldistribution in the core-to-corner middle region.

(2) The isothermal friction factors increase with increasing duct aspect ratio, as well as with increasing flow behavior index n. The exception to this is highly shear-thinning flow ($n \leqslant 0.6$), where maximum fRe_g is obtained for $\gamma = 1$. Friction factors for pseudoplastic fluids ($n < 1$) are much less than those for Newtonian ($n = 1$) flows in double-sine duct with a given γ and the same flow rate; for dilatant fluids ($n > 1$) friction factors are significantly higher.

(3) Reflecting the fluid flow behavior and its rheology, for both **T** and **H1** conditions Nu decreases as n increases, irrespective of the duct aspect ratio. The heat transfer is enhanced in pseudoplastic flows; conversely, lower Nu is obtained in dilatant flows. Furthermore, Nu decreases when $\gamma < 1$ and $\gamma > 1$ for

Table 3. Fully developed laminar power-law fluid flow heat transfer characteristics in double-sine ducts with the **H1** thermal boundary condition

n	0.15	0.40	0.60	0.80	1.00	1.20	1.50	2.00	2.50
					$\gamma = 0.25$				
θ_{max}/θ_b	1.8010	1.7664	1.7542	1.7489	1.7463	1.7449	1.7438	1.7430	1.7424
Nu_{H1}	2.9004	2.5882	2.4596	2.3853	2.3417	2.3132	2.2834	2.2508	2.2324
					$\gamma = 0.50$				
$\theta_{max}/\theta b$	1.7298	1.6957	1.6819	1.6751	1.6709	1.6679	1.6647	1.6614	1.6593
Nu_{H1}	3.0228	2.9419	2.8641	2.8006	2.7517	2.7128	2.6667	2.6100	2.5689
					$\gamma = 1.00$				
θ_{max}/θ_b	1.7143	1.6947	1.6817	1.6747	1.6703	1.6672	1.6638	1.6602	1.6578
Nu_{H1}	3.8217	3.5464	3.4318	3.3741	3.3203	3.2729	3.2124	3.1328	3.0717
					$\gamma = 2.00$				
θ_{max}/θ_b	1.8326	1.8113	1.7916	1.7774	1.7682	1.7623	1.7572	1.7534	1.7522
Nu_{H1}	3.6231	3.4697	3.3697	3.2717	3.2042	3.1551	3.1019	3.0430	3.0036
					$\gamma = 4.00$				
θ_{max}/θ_b	2.1034	2.0214	1.9685	1.9406	1.9293	1.9261	1.9251	1.9244	1.9235
Nu_{H1}	3.5044	2.8411	2.8274	2.8007	2.7484	2.7258	2.7173	2.6870	2.5911

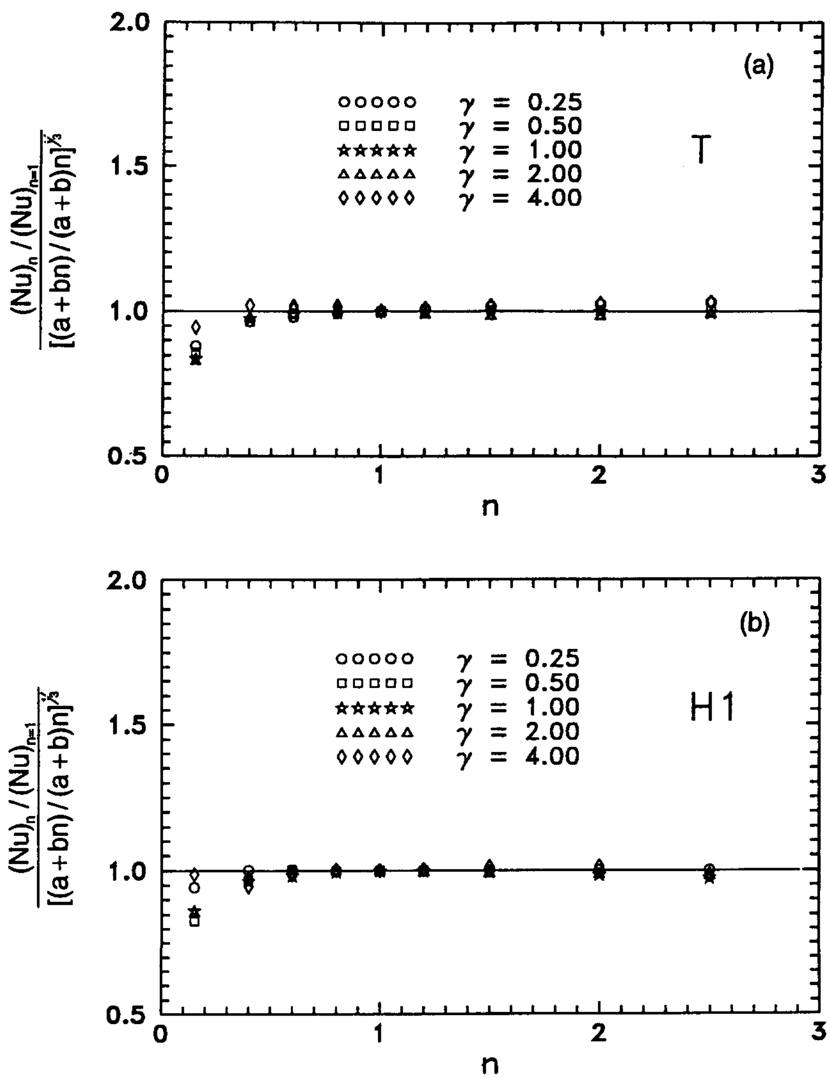

Fig. 7. Effectiveness of Cheng [13] parameter for correlating Nu in double-sine ducts: (a) for **T** and (b) for **H1** boundary conditions.

both **T** and **H1** conditions, with the peak heat transfer performance for $\gamma \approx 1$. For all cases of γ and n, however, consistent with the effects of wall thermal conditions, $Nu_{H1} > Nu_T$.

(4) The correlating parameters proposed by Kozicki *et al.* [22] for fRe^* and by Cheng [13] for Nu are found to give reasonable first order estimates in most cases. While the heat transfer predictions are in excellent agreement with results for all γ and n (except $n = 0.15$), the friction factor results correlate well only for near unity values of n and γ. More generalized predictions of non-Newtonian flow and heat transfer in irregular shaped ducts perhaps require modified strategies.

Acknowledgements—This study was supported in part by the National Science Foundation CAREER award (Grant no. CTS 9502128) and by Procter & Gamble.

REFERENCES

1. Shah, R. K. and London, A. L., Laminar flow forced convection in ducts, Suppl. 1. In *Advances in Heat Transfer*, ed. T. F. Irvine, Jr and J. P. Hartnett. Academic, New York, 1978.
2. Bergles, A. E., Techniques to augment heat transfer. In *Handbook of Heat Transfer Applications*, 2nd edn, Chap. 3, ed. W. M. Rohsenow, J. P. Hartnett and E. N. Ganic. McGraw–Hill, New York, 1985.
3. Webb, R. L., *Principles of Enhanced Heat Transfer*. Wiley, New York, 1994.
4. Manglik, R. M. and Muley, A., Heat transfer and pressure drop characteristics of plate-and-frame heat exchangers—a literature review. Report no. TFL-Int-1, Thermal-Fluids Laboratory, University of Cincinnati, Cincinnati, Ohio, 1993.
5. Shah, R. K. and Focke, W. W., Plate heat exchangers and their design theory. In *Heat Transfer Equipment Design*, ed. R. K. Shah, E. C. Subbarao and R. A. Mashelkar. Hemisphere, New York, 1988, pp. 227–254.
6. Bird, R. B., Armstrong, R. C. and Hassager, O., *Dynamics of Polymeric Liquids*, Vol. 1. Wiley, New York, 1977.
7. Cho, Y. I. and Hartnett, J. P., Non-Newtonian fluids in circular pipe flow. In *Advances in Heat Transfer*, Vol. 15, ed. J. P. Hartnett and T. F. Irvine, Jr. Academic, New York, 1982, pp. 59–141.
8. Irvine, Jr T. F. and Karni, J., Non-Newtonian fluid flow and heat transfer. In *Handbook of Single Phase Convective Heat Transfer*, Chap. 20, ed. S. Kakaç, R. K. Shah and W. Aung. Wiley, New York, 1987.
9. Bergles, A. E., Effects of temperature-dependent properties on non-Newtonian flows. In *Low Reynolds Number Flow Heat Exchangers*, ed. S. Kakaç, R. K. Shah and A. E. Bergels. Hemisphere, Washington, 1983, pp. 593–612.
10. Herwig, H. and Körber, J., An asymmptotic theory for laminar pipe flow of a non-Newtonian fluid. *Wärme- und Stoffübertragung*, 1989, **24**, 87–95.
11. Prusa, J. and Manglik, R. M., Asymptotic and numerical solutions for thermally developing flows of Newtonian fluids in circular tubes with uniform wall temperature. *Numerical Heat Transfer, Part A*, 1994, **26**, 199–217.
12. Manglik, R. M. and Prusa, J., Viscous dissipation in non-Newtonian flows: implications for the Nusselt number. *Journal of Thermophysics and Heat Transfer*, 1995, **9**, 733–742.
13. Cheng, J.-A., Laminar forced convective heat transfer of power-law fluids in isosceles triangular ducts with peripheral wall conduction. Ph.D. thesis, Department of Mechanical Engineering, State University of New York at Stony Brook, New York, 1984.
14. Capobianchi, M. and Irvine, Jr T. F., Predictions of pressure drop and heat transfer in concentric annular ducts with modified power-law fluids. *Wärme- und Stoffübertragung*, 1992, **27**, 209–215.
15. Gingrich, W. K., Cho, Y. I. and Shyy, W., Effects of shear thinning on laminar heat transfer behavior in a rectangular duct. *International Journal of Heat and Mass Transfer*, 1992, **35**, 2823–2836.
16. Hartnett, J. P. and Kostic, M., Heat Transfer to Newtonian and non-Newtonian fluids in rectangular ducts. In *Advances in Heat Transfer*, Vol. 19, ed. J. P. Hartnett and T. F. Irvine, Jr. Academic, New York, 1989, pp. 247–356.
17. Etemad, S. Gh., Mujumdar, A. S. and Huang, B., Laminar forced convection heat transfer of a non-Newtonian fluid in the entrance region of a square duct with different boundary conditions. In *Heat Transfer* 1994, Vol. 4, ed. G. F. Hewitt. I.Chem.E., U.K., 1994, pp. 231–236.
18. Chandrupatla, A. R. and Sastri, V. M. K., Laminar forced convection heat transfer of a non-Newtonian fluid in a square duct. *International Journal of Heat and Mass Transfer*, 1977, **20**, 1315–1324.
19. Lawal, A. and Mujumdar, A. S., Laminar flow and heat transfer in power-law fluids flowing in arbitrary cross-sectional ducts. *Numerical Heat Transfer, Part A*, 1985, **8**, 217–244.
20. Etemad, S. Gh. and Mujumdar, A. S., Effects of variable viscosity and viscous dissipation on laminar convection heat transfer of a power law fluid in the entrance region of a semi-circular duct. *International Journal of Heat and Mass Transfer*, 1995, **38**, 2225–2238.
21. Etemad, S. Gh., Laminar heat transfer to viscous non-Newtonian fluids in non-circular ducts. Ph.D. thesis, Department of Chemical Engineering, McGill University, Montreal, QB, 1995.
22. Kozicki, W., Chou, C. H. and Tiu, C., Non-Newtonian flow in ducts of arbitrary cross-sectional shape. *Chemical Engineering Science*, 1966, **21**, 665–679.
23. Miller, C., Predicting non-Newtonian flow behavior in ducts of unusual cross section. *Industrial Engineering Chemistry Fundamentals*, 1972, **11**, 524–528.
24. Kantorovich, L. V. and Krylov, V. I., *Approximate Methods of Higher Analysis*. Interscience, New York, 1964.
25. Payne, F. P., Corduneau, C. C., Haji-Sheikh, A. and Huang, T., *Integral Methods in Science and Engineering*. Hemisphere, Washington, 1986.
26. Haji-Sheikh, A., Mashena, M. and Haji-Sheikh, M. J., Heat transfer coefficient in ducts with constant wall temperature. *Journal of Heat Transfer*, 1983, **105**, 878–883.
27. Lakshminarayanan, R. and Haji-Sheikh, A., Extended Graetz problems in irregular ducts. In *Proceedings of the 1988 National Heat Transfer Conference*, HTD-96, Vol. 1, ed. H. R. Jacobs. ASME, New York, 1988, pp. 475–482.
28. Ding, J. and Manglik, R. M., Analytical solutions for laminar fully developed flows in double-sine shaped ducts. *Heat and Mass Transfer*, 1996, **31**, 269–277.
29. Ding, J., Integral solutions for laminar fully developed non-Newtonian flows in irregular ducts. M.S. thesis, Department of Mechanical, Industrial and Nuclear Engineering, University of Cincinnati, Cincinnati, OH, 1995.